

Article

Comprehensive Evidence of Carrier-Mediated Distribution of Amantadine to the Retina across the Blood–Retinal Barrier in Rats

Yusuke Shinozaki, Shin-ichi Akanuma , Yuika Mori, Yoshiyuki Kubo and Ken-ichi Hosoya * 

Department of Pharmaceutics, Graduate School of Medicine and Pharmaceutical Sciences, University of Toyama, 2630 Sugitani, Toyama 930-0194, Japan; m2061220@ems.u-toyama.ac.jp (Y.S.); akanumas@pha.u-toyama.ac.jp (S.-i.A.); s1860308@ems.u-toyama.ac.jp (Y.M.); kubo.yoshiyuki.jf@teikyo-u.ac.jp (Y.K.)

* Correspondence: hosoyak@pha.u-toyama.ac.jp; Tel.: +81-76-434-7505

Abstract: Amantadine, a drug used for the blockage of NMDA receptors, is well-known to exhibit neuroprotective effects. Accordingly, assessment of amantadine transport at retinal barriers could result in the application of amantadine for retinal diseases such as glaucoma. The objective of this study was to elucidate the retinal distribution of amantadine across the inner and outer blood–retinal barrier (BRB). In vivo blood-to-retina [³H]amantadine transport was investigated by using the rat retinal uptake index method, which was significantly reduced by unlabeled amantadine. This result indicated the involvement of carrier-mediated processes in the retinal distribution of amantadine. In addition, in vitro model cells of the inner and outer BRB (TR-iBRB2 and RPE-J cells) exhibited saturable kinetics (K_m in TR-iBRB2 cells, 79.4 μ M; K_m in RPE-J cells, 90.5 and 9830 μ M). The inhibition of [³H]amantadine uptake by cationic drugs/compounds indicated a minor contribution of transport systems that accept cationic drugs (e.g., verapamil), as well as solute carrier (SLC) organic cation transporters. Collectively, these outcomes suggest that carrier-mediated transport systems, which differ from reported transporters and mechanisms, play a crucial role in the retinal distribution of amantadine across the inner/outer BRB.

Keywords: amantadine; blood–retinal barrier; drug delivery; retinal disease; NMDA receptor; inner BRB; retinal capillary endothelial cells; outer BRB; retinal pigment epithelial cells; transporter



Citation: Shinozaki, Y.; Akanuma, S.-i.; Mori, Y.; Kubo, Y.; Hosoya, K.-i. Comprehensive Evidence of Carrier-Mediated Distribution of Amantadine to the Retina across the Blood–Retinal Barrier in Rats. *Pharmaceutics* **2021**, *13*, 1339. <https://doi.org/10.3390/pharmaceutics13091339>

Academic Editor: Gert Fricker

Received: 12 July 2021

Accepted: 24 August 2021

Published: 26 August 2021

Publisher's Note: MDPI stays neutral with regard to jurisdictional claims in published maps and institutional affiliations.



Copyright: © 2021 by the authors. Licensee MDPI, Basel, Switzerland. This article is an open access article distributed under the terms and conditions of the Creative Commons Attribution (CC BY) license (<https://creativecommons.org/licenses/by/4.0/>).

1. Introduction

Retinal neurodegenerative diseases, such as glaucoma and diabetic retinopathy, cause progressive visual deficit [1,2]. It is well-known that the progression of the visual deficit involves N-methyl-D-aspartate (NMDA) receptors [3,4]. Previous in vitro and in vivo analyses have indicated the involvement of overactivation of NMDA receptors in the loss of retinal ganglion cells (RGCs) [5,6], which transmit light stimuli from the eye to the brain. Recently, there has been an attempt to block NMDA receptors for the treatment of retinal diseases. For example, it has been reported that memantine, which is an adamantane derivative and an inhibitor of NMDA receptors, has been shown to exhibit neuroprotection in the retina of animal models of retinal diseases, both in vitro and in vivo [7,8]. Moreover, pharmacotherapy with memantine for glaucoma has reached phase III clinical trials [9]. Although a clinical trial of memantine failed [10], it is believed that adamantane derivatives have the potential to treat retinal diseases. Among the adamantane derivatives that are utilized for the blockage of NMDA receptors in clinical practice, amantadine shows the simplest structure. Therefore, scrutiny of the manner of retinal amantadine distribution could contribute to the clinical application of these derivatives.

The blood–retinal barrier (BRB) is known to regulate retinal drug distribution and is composed of retinal capillary endothelial and pigmented epithelial cells, termed the inner

BRB and outer BRB, respectively [11]. Although the paracellular transport of compounds across these barriers is restricted by cellular tight junctions, recent studies have suggested that several ionic nutrients and drugs are supplied by blood-to-retina transport mediated by various plasma membrane transporters and transport systems [12]. As the pKa value of amantadine is 10.1, it is indicated that amantadine exists in the cationic form under physiological conditions (pH ~7.4) [13]. Accordingly, to develop a suitable strategy for efficient retinal amantadine distribution, an understanding of the retinal distribution of amantadine across the BRB would be valuable, in addition to clarifying the involvement of plasma membrane transport systems during this process.

To date, several solute carrier (SLC) transporters have been identified in amantadine transport in vivo and in vitro. As shown in Table 1, the roles of multidrug and toxin extrusion protein 1 (MATE1/Slc47a1) and neutral and basic amino acid transporter (ATB^{0,+}/Slc6a14) at several tissues in amantadine transport have been reported [14,15]. Moreover, amantadine is reportedly a substrate for SLC organic cation transporter 1, abbreviated as OCT1 (Slc22a1), and OCT2 (Slc22a2) [16,17]. Among these transporters, mRNA expression of MATE1 has been observed in the inner and outer BRB model cells [18,19]. In addition to MATE1, the expression of other organic cation transporter subtypes has been documented. For example, plasma membrane monoamine transporter (PMAT/slc29a4) and organic cation/L-carnitine transporters 1-2 (OCTN1-2/slc22a4-5) are expressed at the BRB [18,19]. Moreover, putative cationic drug transport systems that accept several cationic and lipophilic drugs, including verapamil, clonidine, and propranolol, are known to exist in the inner BRB [20–23]. In these previous reports, amantadine reportedly exhibited an inhibitory effect on the uptake of these cationic drugs in inner BRB model cells, namely TR-iBRB2 cells [24]. Based on these lines of evidence, it can be speculated that these transporters and putative transport systems at the inner and outer BRB participate in amantadine transport to the retina across the BRB.

The present study aimed to clarify the details underlying the retinal distribution of amantadine. Herein, we used the retinal uptake index (RUI) experiment to elucidate the role of carrier-mediated processes in the retinal transfer of amantadine. In addition, the properties of amantadine transport across the inner and outer BRB were determined by using TR-iBRB2 cells and a conditionally immortalized rat RPE cell line (RPE-J cells) [25].

Table 1. Candidates of amantadine transporter and transport system in the retina.

Name		Is Amantadine Accepted as a Substrate?	Is It Expressed in the Retina?
Slc6a14	ATB ^{0,+}	Yes [15]	N.D.
Slc22a1	OCT1	Yes [16]	N.D.
Slc22a2	OCT2	Yes [17]	N.D.
Slc22a3	OCT3	N.D.	N.D.
Slc22a4	OCTN1	N.D.	Yes (mRNA) [18]
Slc22a5	OCTN2	N.D.	Yes (mRNA) [18]
Slc29a4	PMAT	N.D.	Yes (mRNA) [19]
Slc47a1	MATE1	Yes [14]	Yes (mRNA) [19]
Putative transport systems	Verapamil Clonidine Propranolol	N.D.	Yes [20–23]

N.D., not determined.

2. Materials and Methods

2.1. Animals and Reagents

The animal experiments performed in this study were approved by the Animal Care Committee of the University of Toyama with the registration numbers of A2017PHA-6 and A2020PHA-1. Male Wistar/ST rats (approximately 200 g; Japan SLC, Hamamatsu, Japan) were maintained under controlled conditions (12/12 h dark/light cycle; temperature, ~23 °C; humidity, around 50%). Male rats present an advantage for the comparison of

previous reports of in vivo retinal distribution, as quantitative data of compound distribution to the retina have been obtained by using male rats [26]. A total of 13 rats were used for the assessment of in vivo blood-to-retina transport (control, $n = 5$; co-administration of unlabeled amantadine, $n = 4$; co-administration of PAH, $n = 4$). Amantadine HCl, [^3H]- ([^3H]amantadine; 0.3 Ci/mmol) was obtained from Moravek (Brea, CA, USA). From American Radiolabeled Chemicals (St. Louis, MO, USA), n -[^{14}C]butanol ([^{14}C]n-butanol; $2.0 \times 10^3 \mu\text{Ci/mmol}$) and verapamil [N-methyl- ^3H] hydrochloride ([^3H]verapamil; 80 Ci/mmol) were purchased. Unlabeled drugs and compounds used in this study were commercially available.

2.2. Assessment of In Vivo Blood-to-Retina Transport

Rats were anesthetized by an intraperitoneal injection of pentobarbital sodium at 50 mg/kg. Using the rats, intracarotid artery injection was performed by following the method given in previous manuscripts [20–22,26], and the details of the procedure are given in the Supplementary Materials. The functional retinal compound distribution as a percentage of the in vivo retinal transfer of [^{14}C]n-butanol (RUI) was determined by using Equation (1).

$$\text{RUI (\%)} = ([^3\text{H}]\text{amantadine}/[^{14}\text{C}]n\text{-butanol (in retina)})/([^3\text{H}]\text{amantadine}/[^{14}\text{C}]n\text{-butanol (in the injected solution)}) \times 100 \quad (1)$$

2.3. In Vitro Transport Study

In 10% fetal bovine serum (FBS; Merck, Darmstadt, Germany)-containing Dulbecco's modified Eagle's medium (DMEM; Nissui Pharmaceutical, Tokyo, Japan) with 20 mM NaHCO_3 , 0.19 mM benzylpenicillin potassium, and 0.14 mM streptomycin sulfate, TR-iBRB2 cells (passage number 32–60) were cultured according to previous reports [20–22,24]. As described previously [25,27], RPE-J cells (passage number 79–92) were cultured in DMEM with 4% FBS, 20 mM NaHCO_3 , and 0.1 mM non-essential amino acid (FUJIFILM Wako Pure Chemical, Osaka, Japan) containing 0.16 mM benzylpenicillin potassium and 0.17 mM streptomycin sulfate. In accordance with established protocols for the uptake study [20–22], the cells were seeded at a density of 1.0×10^5 cells/well onto a collagen I-coated 24-well plate (BioCoat™ Collagen I Cellware, Corning, Corning, NY, USA) and cultured for 2 days, at 33 °C, under 5% CO_2 /air. Referring to the previous reports [20–23,28,29], we started the uptake reaction, and the details of the procedure are included in the Supplemental Materials.

The uptake activities for [^3H]amantadine and [^3H]verapamil were calculated as the cell/medium ratio, using Equation (2).

$$\text{Cell/medium ratio} = [^3\text{H}]\text{compound (dpm) per cell protein (mg)}/[^3\text{H}]\text{compound (dpm) per medium (\mu\text{L})} \quad (2)$$

Kinetic parameters for cell uptake, such as the maximal uptake rate (V_{\max}), Michaelis–Menten constant (K_m), and non-saturable uptake clearance (K_d), were obtained by using the nonlinear least-squares regression analysis program (MULTI) [30] with Equations (3)–(5), where the uptake rate of the test compound and its concentration were V and S , respectively.

$$V = (V_{\max} \times S)/(K_m + S) \quad (3)$$

$$V = (V_{\max} \times S)/(K_m + S) + K_d \times S \quad (4)$$

$$V = (V_{\max 1} \times S)/(K_{m1} + S) + (V_{\max 2} \times S)/(K_{m2} + S) \quad (5)$$

2.4. Data and Statistical Analyses

All the data are shown as the mean \pm standard deviation (SD). Using the unpaired two-tailed Student's t -test (two groups) or one-way analysis of variance followed by Dunnett's test (more than two groups), statistical differences were evaluated.

3. Results

3.1. In Vivo Blood-to-Retina Transport of [^3H]Amantadine across the BRB

The in vivo RUI was observed to be $129 \pm 13\%$ (Figure 1), indicating that retinal distribution of [^3H]amantadine is 1.29-fold greater than that of [^{14}C]n-butanol. Following co-administration of 50 mM unlabeled amantadine, the RUI value significantly decreased by 44%. To test the effect of compounds at the same concentration, co-administration of 50 mM p -aminohippuric acid (PAH),

which is an anionic compound that is reported to have no effect on the retinal distribution of cationic drugs, such as propranolol and clonidine [21,22], was performed. As a result, no significant effect was observed in the presence of 50 mM PAH (Figure 1).

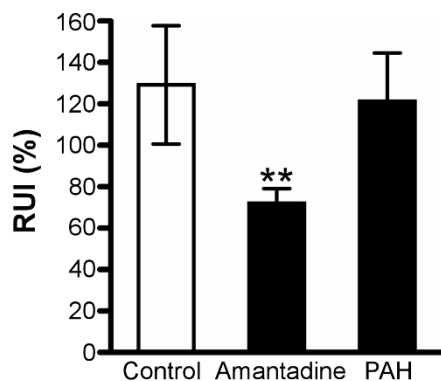


Figure 1. [^3H]Amantadine RUI in rats. [^3H]Amantadine ($5\ \mu\text{Ci}/\text{rat}$) and [^{14}C]n-butanol ($0.5\ \mu\text{Ci}/\text{rat}$) were injected in the absence (control, $n = 5$) or presence of 50 mM unlabeled amantadine ($n = 4$) or 50 mM PAH ($n = 4$). Each column, expressing [^3H]amantadine RUI, represents the mean \pm SD; ** $p < 0.01$, significant difference from control. RUI, retinal uptake index; PAH, *p*-aminohippuric acid.

3.2. Amantadine Uptake Properties in TR-iBRB2 Cells

TR-iBRB2 cells showed a time-dependent increase in [^3H]amantadine uptake for at least 5 min. The initial uptake rate was presented as $14.0 \pm 4.1\ \mu\text{L}/(\text{min}\cdot\text{mg}\ \text{protein})$ (Figure 2A). At $4\ ^\circ\text{C}$, the [^3H]amantadine uptake significantly reduced by 86% (Figure 2A). Concentration-dependent uptake of amantadine by TR-iBRB2 cells exhibited saturable and non-saturable processes, with a V_{max} of $1.36 \pm 0.38\ \text{nmol}/(\text{min}\cdot\text{mg}\ \text{protein})$, a K_m of $79.4 \pm 27.3\ \mu\text{M}$, and a K_d of $2.75 \pm 0.58\ \mu\text{L}/(\text{min}\cdot\text{mg}\ \text{protein})$ (Figure 2B).

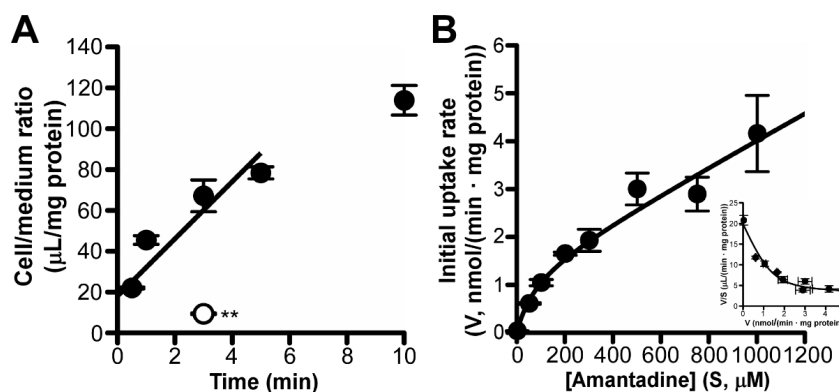


Figure 2. Time-, temperature-, and concentration-dependent uptake of [^3H]amantadine by TR-iBRB2 cells. (A) Time dependency of [^3H]amantadine uptake ($1.67\ \mu\text{M}$, $0.1\ \mu\text{Ci}/\text{well}$) by TR-iBRB2 cells at $37\ ^\circ\text{C}$ (control; closed circles) and effect of low temperature ($4\ ^\circ\text{C}$; open circle) on the uptake; ** $p < 0.01$, significant difference from the control. (B) Concentration dependency of amantadine uptake by TR-iBRB2 cells. Amantadine uptake was examined at $37\ ^\circ\text{C}$ for 3 min over the concentration range of 1.67 to $1000\ \mu\text{M}$ and analyzed by using Michaelis-Menten and Eadie-Scatchard (inset) plots. Each point in the figure represents the mean \pm SD ($n = 3$).

Furthermore, Na^+ -free and K^+ -replacement buffer had no significant effect on the uptake of [^3H]amantadine by TR-iBRB2 cells; however, Cl^- -free buffer significantly reduced the uptake of [^3H]amantadine by 38% (Figure 3A). At an extracellular pH of 6.4, [^3H]amantadine uptake by TR-iBRB2 cells was significantly reduced by 64% (Figure 3B). At an extracellular pH of 8.4, we noted the tendency of an increase in uptake of [^3H]amantadine by TR-iBRB2 cells (Figure 3B). A proton ionophore, namely carbonyl cyanide-*p*-trifluoromethoxyphenylhydrazone (FCCP) [21,27], significantly decreased uptake by 50% at $50\ \mu\text{M}$ (Figure 3C). In previous studies, it was indicated

the acute treatment and pretreatment of NH_4Cl caused alkalinized and acidified intracellular pH in endothelial and epithelial cells, respectively [28,29]. Although acute NH_4Cl treatment also induces the neutralization between the acid endosomal/lysosomal and intracellular compartments [27], we performed a study of [^3H]amantadine uptake with acute and pretreatment of NH_4Cl to examine the effect of H^+ -gradient on the intra- and extra-cellular compartments. The uptake was significantly decreased by 80% and increased by 90% at alkalinized and acidified intercellular pH, respectively (Figure 3D). Under the experimental conditions in Figure 3, there is a possibility that the cytotoxicity may have affected the results of this uptake, because these experimental conditions are not ideal for the culture of these cells. However, the cellular protein amount after the uptake reaction was not significantly altered in each group compared with the control (Supplementary Materials Figure S1). Therefore, the cytotoxic effect caused by these experimental conditions is considered to be minimal.

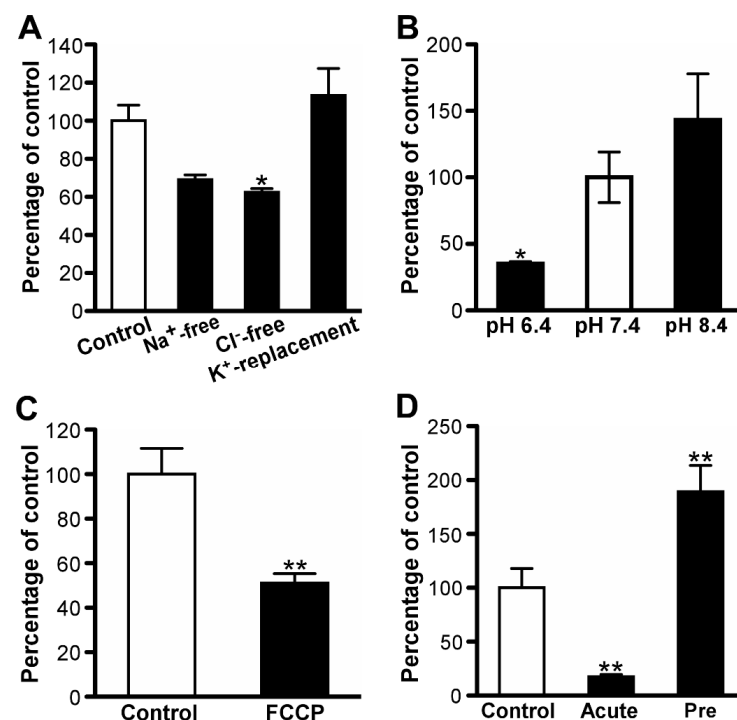


Figure 3. Uptake properties of [^3H]amantadine by TR-iBRB2 cells. (A) Effect of Na^+ , Cl^- , and membrane potential on [^3H]amantadine uptake (1.67 μM , 0.1 $\mu\text{Ci}/\text{well}$) for 3 min at 37 $^\circ\text{C}$. (B) Effect of extracellular pH on [^3H]amantadine uptake by TR-iBRB2 cells. (C) Effect of carbonyl cyanide-*p*-trifluoromethoxyphenylhydrazone (FCCP) treatment at 50 μM on [^3H]amantadine uptake. (D) Effect of intracellular pH on the uptake of [^3H]amantadine for 15 s by TR-iBRB2 cells at 37 $^\circ\text{C}$. Pretreatment (Pre) and acute treatment with 30 mM NH_4Cl were performed to decrease and increase intracellular pH, respectively. Each column in the figure represents the mean \pm SD ($n = 3$); * $p < 0.05$, ** $p < 0.01$, significantly different from the control.

3.3. Amantadine Uptake Properties in RPE-J Cells

In the current study, [^3H]amantadine was time-dependently incorporated for at least 3 min in RPE-J cells, at an initial uptake rate of $15.9 \pm 0.3 \mu\text{L}/(\text{min}\cdot\text{mg protein})$ (Figure 4A). At 4 $^\circ\text{C}$, this uptake was significantly reduced by 87% (Figure 4A). Amantadine uptake by RPE-J cells involved both high- and low-affinity saturable processes (Figure 4B). Following the calculation, K_{m1} and V_{max1} values were $90.5 \pm 49.6 \mu\text{M}$ and $0.914 \pm 0.510 \text{ nmol}/(\text{min}\cdot\text{mg protein})$, respectively, for the high-affinity uptake process. For the low-affinity uptake process, the K_{m2} and V_{max2} values were $9830 \pm 1620 \mu\text{M}$ and $85.3 \pm 11.4 \text{ nmol}/(\text{min}\cdot\text{mg protein})$, respectively.

Na^+ -free, Cl^- -free, and K^+ -replacement buffers had no significant impact on the uptake of [^3H]amantadine by RPE-J cells (Figure 5A). The uptake of [^3H]amantadine by RPE-J cells was significantly decreased by 32% and increased by 25% at extracellular pH of 6.4 and 8.4, respectively (Figure 5B). Furthermore, the uptake of [^3H]amantadine by RPE-J cells was significantly decreased by 78% and increased by 18% at alkalinized and acidified intercellular pH, respectively (Figure 5C). The

cellular protein in each group of Figure 5 also had no significant difference compared with control (Supplementary Materials Figure S2).

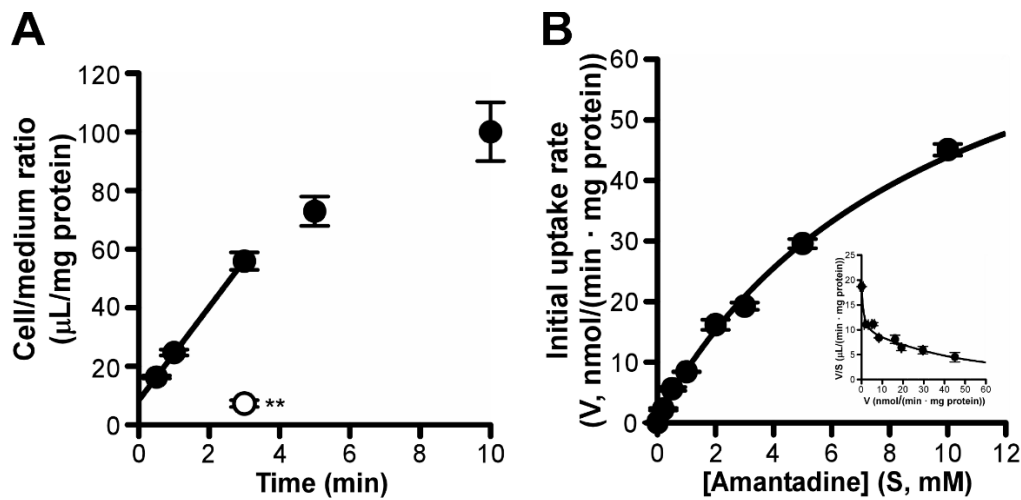


Figure 4. Time-, temperature-, and concentration-dependent uptake of [³H]amantadine by RPE-J cells. (A) Time dependency of [³H]amantadine uptake (1.67 μM, 0.1 μCi/well) by RPE-J cells (37 °C; control, closed circles) and effect of low temperature (4 °C; open circle) on [³H]amantadine uptake; ** *p* < 0.01, significant difference from the control. (B) Concentration-dependent uptake of amantadine (1.67 μM–10 mM) by RPE-J cells was expressed by using Michaelis-Menten and Eadie-Scatchard (inset) plots. Each point in the figure represents the mean ± SD (*n* = 3).

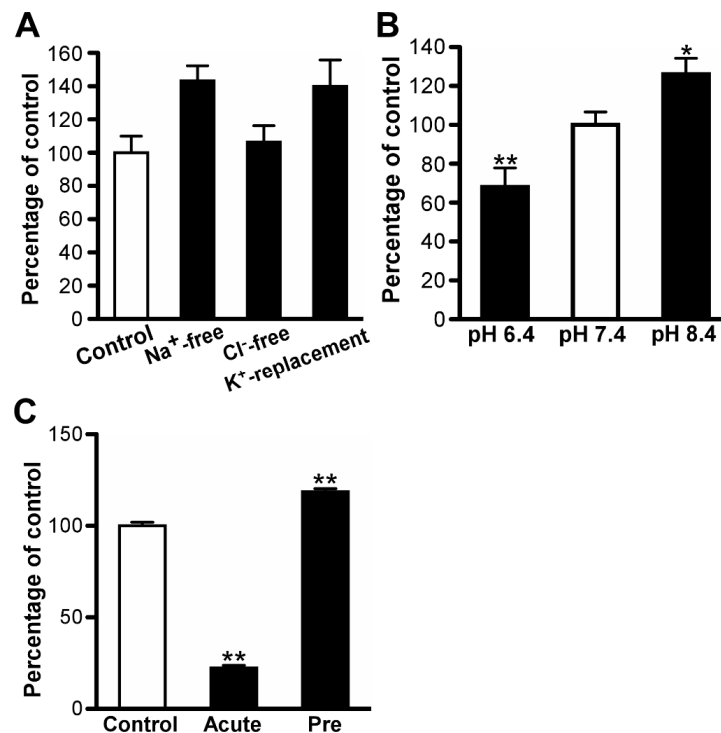


Figure 5. Properties of [³H]amantadine uptake by RPE-J cells. (A) Effect of Na⁺, Cl⁻, and membrane potential on [³H]amantadine uptake (1.67 μM, 0.1 μCi/well) for 3 min at 37 °C. (B) Effect of extracellular pH on the uptake of [³H]amantadine. (C) Effect of intracellular pH on [³H]amantadine uptake for 15 s at 37 °C by RPE-J cells. Pretreatment (Pre) and acute treatment with 30 mM NH₄Cl were performed to decrease and increase intracellular pH, respectively. Each column in the figure represents the mean ± SD (*n* = 3); * *p* < 0.05, ** *p* < 0.01, significantly different from the control.

3.4. Inhibition of [³H]Amantadine Transport by Drugs/Compounds

The inhibitory effects on the in vitro [³H]amantadine uptake are summarized in Table 2. At 0.2 mM, several cationic drugs (desipramine, imipramine, quinidine, and verapamil) strongly inhibited [³H]amantadine uptake by both TR-iBRB2 cells and RPE-J cells.

Table 2. Effect of compounds on the uptake of [³H]amantadine by TR-iBRB2 cells and RPE-J cells.

Compound	Concentration (mM)	% of Control	
		TR-iBRB2	RPE-J
Control		100 ± 12	100 ± 12
Desipramine	0.2	7.05 ± 0.57 **	10.7 ± 5.6 **
Imipramine	0.2	8.37 ± 1.43 **	16.9 ± 5.2 **
Propranolol	0.2	8.61 ± 0.75 **	15.7 ± 5.9 **
Quinidine	0.2	13.7 ± 1.8 **	34.1 ± 3.0 **
Memantine	0.2	16.7 ± 2.2 **	123 ± 38 **
	1.0	N.D.	27.1 ± 2.6 **
Pyrilamine	0.2	20.9 ± 1.8 **	77.8 ± 38.4
	1.0	N.D.	18.2 ± 1.7 **
Verapamil	0.2	22.1 ± 6.2 **	20.5 ± 4.8 **
Amantadine	0.2	34.1 ± 4.1 **	89.9 ± 5.6
	1.0	N.D.	21.3 ± 3.1 **
Timolol	0.2	34.6 ± 10.6 **	59.1 ± 5.1
Clonidine	0.2	42.1 ± 12.1 **	71.6 ± 4.7
	1.0	N.D.	30.8 ± 4.0 **
Pyrimethamine	0.2	44.3 ± 8.8 **	88.9 ± 3.3
PAH	0.2	85.8 ± 10.8	139 ± 33
Acetazolamide	0.2	90.9 ± 3.8	N.D.
Gluconate	0.2	91.7 ± 21.7	86.2 ± 23.4
Cimetidine	0.2	97.6 ± 24.7	106 ± 5
Choline	0.2	101 ± 8	124 ± 39
MPP ⁺	0.2	106 ± 31	75.5 ± 5.0
	1.0	N.D.	91.9 ± 5.6
Decynium-22	0.2	106 ± 31	86.7 ± 41.9
	0.5	N.D.	136 ± 8
L-Carnitine	0.2	111 ± 35	95.1 ± 5.2
	2.5	99.5 ± 2.3	119 ± 28
TEA	0.2	117 ± 45	87.7 ± 11.8
	1.0	N.D.	81.8 ± 10.3
Serotonin	0.2	126 ± 60	158 ± 52 **
L-Glutamic acid	2.5	80.2 ± 10.0	84.5 ± 16.4
L-Aspartic acid	2.5	101 ± 23	79.5 ± 12.7
Glycine	2.5	102 ± 4	116 ± 13
L-Leucine	2.5	112 ± 17	113 ± 16
L-Arginine	2.5	127 ± 15	150 ± 38 **

Uptake of [³H]amantadine (1.67 μM, 0.1 μCi/well) by the indicated cells was performed for 3 min at 37 °C. Each value represents the mean ± SD (*n* = 3–30); ** *p* < 0.01, significantly different from the control. PAH, *p*-aminohippuric acid; MPP⁺, 1-methyl-4-phenylpyridinium; TEA, tetraethylammonium; N.D., not determined.

Memantine, pyrilamine, amantadine, and clonidine (0.2 mM) exhibited a marked inhibition of [³H]amantadine uptake by TR-iBRB2 cells but not RPE-J cells; however, these cationic drugs significantly inhibited [³H]amantadine uptake by RPE-J cells at 1 mM. SLC organic cation/anion transporter substrates, such as PAH, cimetidine, choline, 1-methyl-4-phenylpyridinium (MPP⁺), and decynium-22, did not suppress [³H]amantadine uptake. Similarly, anionic and cationic amino acids, including L-glutamic acid and L-arginine, did not significantly impact [³H]amantadine uptake.

3.5. Mutual Effect of Amantadine and Verapamil on Uptake by TR-iBRB2 Cells

We next examined the involvement of verapamil-sensitive putative transport systems in the inner BRB [20] in amantadine transport. Accordingly, we performed a kinetic analysis of amantadine uptake by TR-iBRB2 cells in the presence of verapamil. On analyzing the Lineweaver–Burk plot, the fitted line of concentration-dependent amantadine uptake by TR-iBRB2 cells in the presence of 10 μM verapamil did not intersect with that in the absence of verapamil, on both the *y*-axis and *x*-axis

(Figure 6A). In the presence of amantadine at 220 μM , the fitted line of concentration-dependent verapamil uptake intersected at the y -axis with that in the absence of amantadine (Figure 6B); this indicated that amantadine competitively inhibits verapamil-sensitive transport mechanisms at the inner BRB.

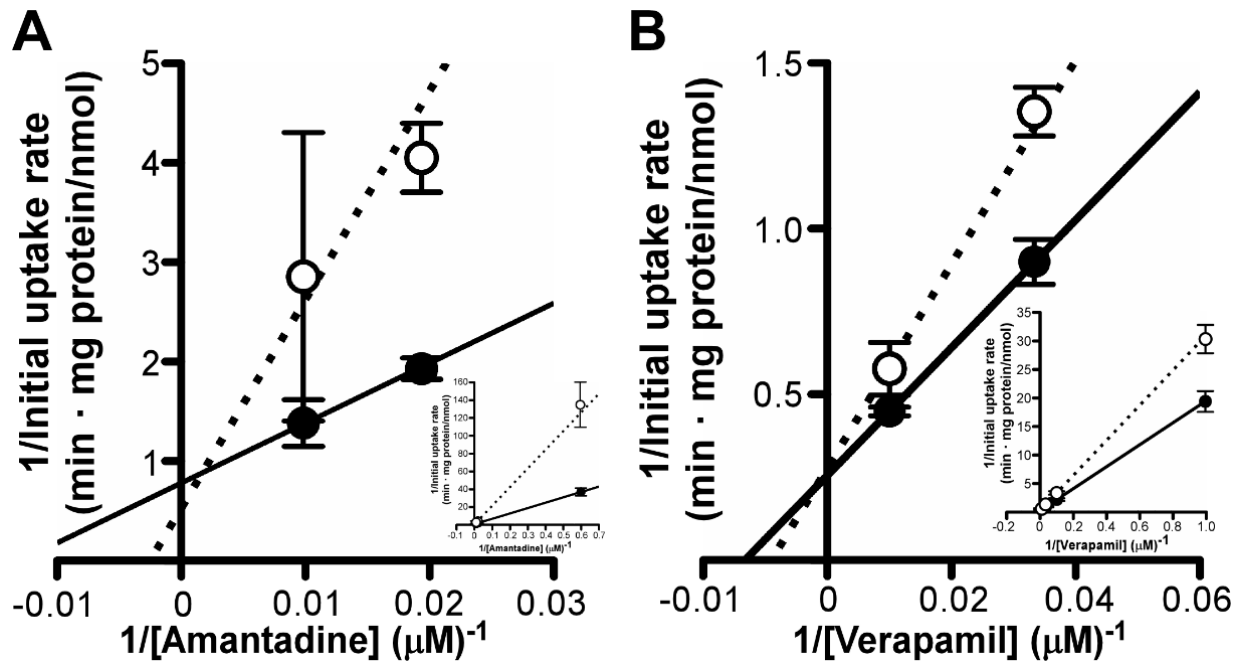


Figure 6. Mutual effect on uptake by TR-iBRB2 cells of amantadine (A) and verapamil (B). (A) The uptake of amantadine at a concentration of 1.67, 50, 100, and 300 μM was assessed at 37 $^{\circ}\text{C}$ for 3 min, with (open circles, dotted line) or without (closed circles, solid line) 10 μM verapamil. (B) The uptake of verapamil at a concentration of 1, 10, 100, and 300 μM was examined at 37 $^{\circ}\text{C}$ for 3 min, with (open circles, dotted line) or without (closed circles, solid line) 220 μM amantadine. Each point in the Lineweaver–Burk plot of all data (inset) and highlighted data at the high concentration range represents the mean \pm SD ($n = 3$).

3.6. Effect of Amantadine on Concentration-Dependent Verapamil Uptake by RPE-J Cells

The effect of amantadine on verapamil-sensitive putative transport systems in the outer BRB was investigated. Herein, we investigated the time-dependent uptake of verapamil by RPE-J cells. RPE-J cells showed a time-dependent increase with an initial uptake rate of $70.4 \pm 5.6 \mu\text{L}/(\text{min} \cdot \text{mg protein})$ in [^3H]verapamil uptake for at least 3 min (Figure 7A). At 1 min, this [^3H]verapamil uptake was reduced with 200 μM unlabeled verapamil by 86% (Figure 7A). In RPE-J cells, verapamil uptake exhibited a saturable process, with a V_{max} value of $6.31 \pm 0.35 \text{ nmol}/(\text{min} \cdot \text{mg protein})$ and a K_m value of $55.6 \pm 5.2 \mu\text{M}$ (Figure 7B). In the Lineweaver–Burk plot analysis, the fitted line of concentration-dependent verapamil uptake by RPE-J cells in the presence of 200 μM amantadine did not intersect with that in the absence of verapamil, at both the y -axis and x -axis (Figure 7B); this suggested that amantadine does not competitively or non-competitively inhibit verapamil transport at the outer BRB.

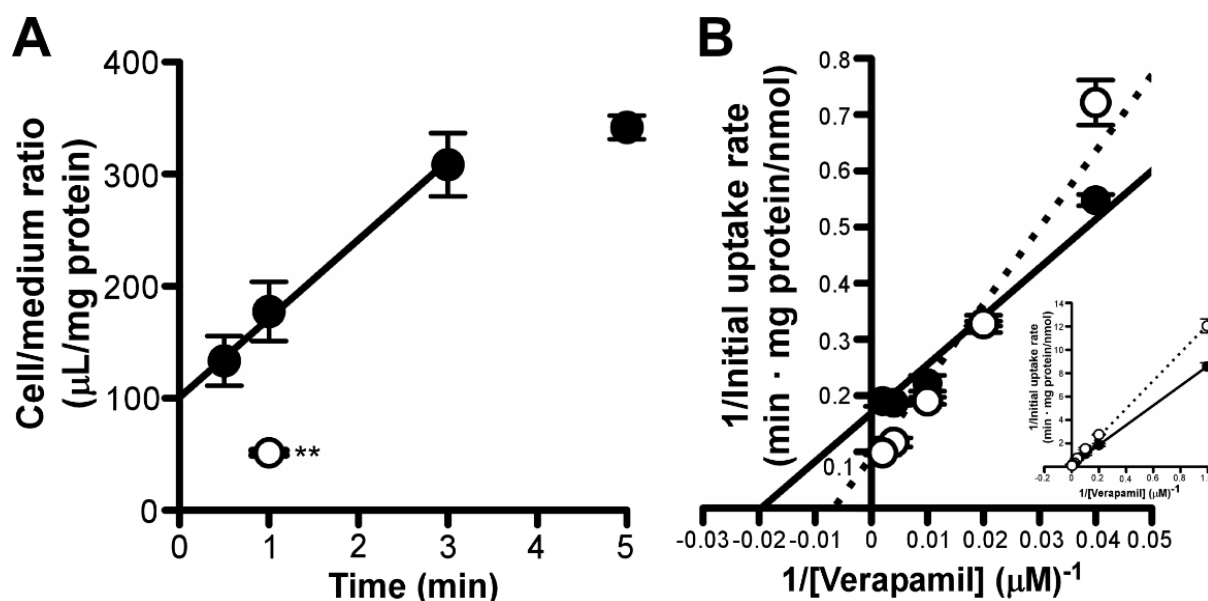


Figure 7. Effects of amantadine on uptake of ^{3}H verapamil by RPE-J cells. (A) Time dependency and self-inhibition of ^{3}H verapamil uptake by RPE-J cells. RPE-J cells were incubated with ^{3}H verapamil (6.25 nM, 0.1 $\mu\text{Ci}/\text{well}$), in the presence (open circle) or absence (control, closed circles) of 200 μM verapamil at 37 $^{\circ}\text{C}$. (B) Lineweaver-Burk plot of all data (inset) and highlighted data at the concentration of 5, 10, 25, 50, 100, 250, and 500 μM verapamil uptake at 37 $^{\circ}\text{C}$ for 3 min, in the absence (closed circles, solid line) or presence (open circles, dotted line) of 100 μM amantadine by RPE-J cells. Each point in the Figure represents the mean \pm SD ($n = 3$); ** $p < 0.01$, significant difference from the control.

4. Discussion

We assessed the inner and outer BRB-mediated transport of amantadine, as well as the carrier-mediated transport of amantadine in the inner and outer BRB. Detailed in vitro analyses clarified characteristics of amantadine transport mechanisms at the BRB; however, the involvement of typical organic cation transporters and putative cationic drug transport systems in the carrier-mediated amantadine transport at the BRB is not suggested.

The in vivo retinal drug transfer study (Figure 1) indicated that amantadine underwent active retinal distribution from the circulating blood. Previously, we reported the correlation between in vivo retinal distribution of drugs transported by passive diffusion and lipophilic properties, indicated as $\log D$ [$\text{RUI} = 46.2 \times \exp(0.515 \times \log D)$] [26]. The $\log D$ value of amantadine is 0.176 [31]. Therefore, if amantadine is only transported to the rat retina by passive diffusion across the in vivo BRB, the RUI value of amantadine can be estimated as 50.4% [$= 46.2 \times \exp(0.515 \times 0.176)$]. Compared with this estimated value, the RUI value of ^{3}H amantadine in the present study was 2.5-fold greater (129%). In addition, unlabeled amantadine at 50 mM showed a significant reduction in the ^{3}H amantadine RUI; however, PAH at the same concentration demonstrated a minimal impact. Based on these findings, it can be suggested that carrier-mediated transport at the inner and outer BRB promotes the retinal distribution of amantadine.

Furthermore, transport studies using in vitro models of the inner and outer BRB detected carrier-mediated amantadine transport at these barriers. In TR-iBRB2 cells, both saturable and non-saturable components were involved in the uptake of amantadine, with a K_m value of 79.4 μM (Figure 2B). As the contribution ratio of the saturable component was 86% [$= V_{\text{max}}/K_m \div (V_{\text{max}}/K_m + K_d) \times 100$], carrier-mediated processes of amantadine uptake could play an important role in amantadine transport at the inner BRB. In terms of the kinetic analysis of amantadine uptake by RPE-J cells, it was observed that this uptake was composed of two saturable processes, with K_m values of 90.5 and 9830 μM for high- and low-affinity processes, respectively (Figure 4B). The contributions of high- and low-affinity processes were calculated as 54% [$= V_{\text{max}1}/K_{m1} \div (V_{\text{max}1}/K_{m1} + V_{\text{max}2}/K_{m2}) \times 100$] and 46% [$= V_{\text{max}2}/K_{m2} \div (V_{\text{max}1}/K_{m1} + V_{\text{max}2}/K_{m2}) \times 100$], respectively; this indicated that the involvement of the high-affinity process in carrier-mediated amantadine transport at the outer BRB is equal to that of the low-affinity process. Collectively, these results suggest that carrier-mediated processes play a major role in amantadine transport across the inner and outer BRB.

As described in the previous section, the K_m value for the saturable process of amantadine uptake by TR-iBRB2 cells (79.4 μM) is similar to that determined for the high-affinity process of

amantadine uptake by RPE-J cells (90.5 μM). However, the contribution ratios of saturable kinetics (50–100 μM) in TR-iBRB2 and RPE-J cells were 86% and 54%, respectively. This difference may influence the properties of net amantadine transport at the inner and outer BRB. For example, TR-iBRB2 cells exhibited Cl^- -sensitive [^3H]amantadine uptake; this effect was not observed in RPE-J cells (Figures 3A and 5A). Moreover, several cationic compounds, such as memantine, pyrillamine, and clonidine, demonstrated a lower inhibitory effect (0.2 mM) on [^3H]amantadine uptake by RPE-J cells than that on uptake by TR-iBRB2 cells (Table 2). The characteristics of high- and low-affinity processes need to be individually evaluated to clarify the differences. Nevertheless, our study, including kinetic analyses, implies that the net transport of amantadine at the inner BRB differs from that at the outer BRB.

Although several transporters reportedly accept amantadine as a substrate, our study indicates a minor contribution of these transporters and putative transport systems in terms of amantadine transport at the inner and outer BRB. We observed no inhibitory effect of OCTs and/or $\text{ATB}^{0,+}$ inhibitors, such as decynium-22, TEA, MPP^+ , glycine, and L-arginine, on [^3H]amantadine uptake by both model cells (Table 2) [32–38]; this indicates that OCTs and $\text{ATB}^{0,+}$ were not involved in amantadine transport at the inner and outer BRB. In addition, typical organic cation transporters that are expressed in the inner and outer BRB, such as OCTN1-2, MATE1, and PMAT, play a minor role in amantadine transport because substrates of these transporters (cimetidine, L-carnitine, TEA, MPP^+ , and serotonin [39–46]) did not significantly reduce [^3H]amantadine uptake by these cells (Table 2). Regarding unidentified cationic drug transport systems for clonidine, propranolol, and verapamil at the BRB [20–22], amantadine transport mechanisms at the inner and outer BRB appear distinct from these cationic drug transport systems based on our results. The K_m values for clonidine and propranolol uptake by TR-iBRB2 cells are 286 and 237 μM , respectively [21,22]. As [^3H]amantadine uptake by TR-iBRB2 cells was reduced by more than 58% in the presence of clonidine and propranolol (0.2 mM), which is lower than the K_m values described above, it is unlikely that putative cationic drug transport systems for clonidine and propranolol participate in amantadine transport at the inner BRB. Reportedly, novel verapamil transport systems have been identified in the rat inner BRB *in vitro* [20]. In addition, the uptake study of verapamil using RPE-J cells indicated the existence of carrier-mediated verapamil transport in the rat outer BRB (Figure 7), as well as human RPE cells [23]. However, it is strongly suggested that amantadine transport systems at the inner and outer BRB are distinct from the verapamil transport systems considering the mutual effect of amantadine and verapamil on uptake by TR-iBRB2 and RPE-J cells (Figures 6A and 7B). Collectively, the results of the functional study suggest that retinal distribution of amantadine across the inner and outer BRB occurs via carrier-mediated transport systems that do not consist of known organic cation transporters and putative organic cation transport systems for cationic drugs, including verapamil.

Parsons et al. reported that amantadine inhibits NMDA receptors, with an IC_{50} of 20 μM [47]. During pharmacotherapy for Parkinson's disease, the plasma concentration range of 0.6–29 μM for amantadine has been established [48]. As the K_m values for the relatively high-affinity process of amantadine transport in the *in vitro* inner and outer BRB model cells (50–100 μM) were greater than the concentrations related to the pharmacology and pharmacetics of amantadine, carrier-mediated amantadine transport at the inner/outer BRB is critical for understanding retinal amantadine distribution. Hence, identifying amantadine transport systems at the BRB could help establish an appropriate pharmaceutical strategy for amantadine applications in retinal diseases. For the identification of the molecule involved in the relatively high-affinity process of amantadine uptake, TR-iBRB2 cells may afford an advantage, as the relatively high-affinity process was the only observed carrier-mediated process of amantadine transport.

5. Conclusions

In the current study, we demonstrated the process of retinal amantadine transport. The RUI experiment indicated the retinal distribution of amantadine. Moreover, the uptake study using *in vitro* model cells suggested the involvement of transport systems in amantadine blood-to-retina transport across the inner and outer BRB. Furthermore, it can be suggested that transport systems for amantadine at the inner/outer BRB are independent of cationic drug transport systems for verapamil, as well as SLC organic cation and amino acid transporters. These transport systems for amantadine at the BRB promote amantadine distribution to the retina. Therefore, the characteristics of amantadine transport at the BRB identified in this study can provide an in-depth understanding of amantadine-sensitive transport mechanisms at the BRB and, thus, the utilization of adamantane derivatives, such as amantadine, for retinal diseases.

Supplementary Materials: The Supplemental Materials are available online at <https://www.mdpi.com/article/10.3390/pharmaceutics13091339/s1>. Figure S1. The cellular protein amount in the group of Figure 3. Each column represents the mean \pm S.D. ($n = 3$). In the tested group, the significant difference from the control was not observed ($p > 0.05$). Figure S2. The cellular protein amount in the group of Figure 5. Each column represents the mean \pm S.D. ($n = 3$). In the tested group, the significant difference from the control was not observed ($p > 0.05$).

Author Contributions: Conception, Y.S., S.-i.A., Y.K. and K.-i.H.; collection, assembly of data, and interpretation, Y.S., S.-i.A. and Y.M.; writing the manuscript, Y.S., S.-i.A. and K.-i.H. All authors have read and agreed to the published version of the manuscript.

Funding: This study was supported by Grant-in-Aids from the Japan Society for Promotion of Science, KAKENHI (Scientific Research (B), 16H05110 and 20H03403; Scientific Research (C), 19K07160).

Institutional Review Board Statement: The animal study was conducted according to the guidelines of the Animal Care Committee of the University of Toyama and approved by the Committee (A2017PHA-6 (date of approval: 14 March 2017) and A2020PHA-1 (date of approval: 9 March 2020)).

Informed Consent Statement: Not applicable.

Data Availability Statement: The data of this study are available from the corresponding author upon reasonable request.

Conflicts of Interest: The authors declare no conflict of interest.

References

1. McMonnies, C.W. Glaucoma history and risk factors. *J. Optom.* **2017**, *10*, 71–78. [[CrossRef](#)]
2. Lechner, J.; O’Leary, O.E.; Stitt, A.W. The pathology associated with diabetic retinopathy. *Vis. Res.* **2017**, *139*, 7–14. [[CrossRef](#)]
3. Fechtner, R.D.; Weinreb, R.N. Mechanisms of optic nerve damage in primary open angle glaucoma. *Surv. Ophthalmol.* **1994**, *39*, 23–42. [[CrossRef](#)]
4. Lipton, S.A. Possible role for memantine in protecting retinal ganglion cells from glaucomatous damage. *Surv. Ophthalmol.* **2003**, *48*, S38–S46. [[CrossRef](#)]
5. Luo, X.; Heidinger, V.; Picaud, S.; Lambrou, G.; Dreyfus, H.; Sahel, J.; Hicks, D. Selective excitotoxic degeneration of adult pig retinal ganglion cells in vitro. *Invest. Ophthalmol. Vis. Sci.* **2001**, *42*, 1096–1106.
6. Chidlow, G.; Osborne, N.N. Rat retinal ganglion cell loss caused by kainate, NMDA and ischemia correlates with a reduction in mRNA and protein of Thy-1 and neurofilament light. *Brain Res.* **2003**, *963*, 298–306. [[CrossRef](#)]
7. Hare, W.A.; Wheeler, L. Experimental glutamatergic excitotoxicity in rabbit retinal ganglion cells: Block by memantine. *Invest. Ophthalmol. Vis. Sci.* **2009**, *50*, 2940–2948. [[CrossRef](#)]
8. Hare, W.; WoldeMussie, E.; Lai, R.; Ton, H.; Ruiz, G.; Feldmann, B.; Wijono, M.; Chun, T.; Wheeler, L. Efficacy and safety of memantine, an NMDA-type open-channel blocker, for reduction of retinal injury associated with experimental glaucoma in rat and monkey. *Surv. Ophthalmol.* **2001**, *45*, S284–S289. [[CrossRef](#)]
9. Weinreb, R.N.; Liebmann, J.M.; Cioffi, G.A.; Goldberg, I.; Brandt, J.D.; Johnson, C.A.; Zangwill, L.M.; Schneider, S.; Badger, H.; Bejani, M. Oral memantine for the treatment of glaucoma: Design and results of 2 randomized, placebo-controlled, phase 3 studies. *Ophthalmology* **2018**, *125*, 1874–1885. [[CrossRef](#)]
10. Bucolo, C.; Platania, C.B.M.; Drago, F.; Bonfiglio, V.; Reibaldi, M.; Avitabile, T.; Uva, M. Novel therapeutics in glaucoma management. *Curr. Neuropharmacol.* **2018**, *16*, 978–992. [[CrossRef](#)]
11. Cunha-Vaz, J.G. The blood-retinal barriers system. Basic concepts and clinical evaluation. *Exp. Eye Res.* **2004**, *78*, 715–721. [[CrossRef](#)]
12. Liu, L.; Liu, X. Roles of drug transporters in blood-retinal barrier. *Adv. Exp. Med. Biol.* **2019**, *1141*, 467–504. [[PubMed](#)]
13. Aoki, F.Y.; Sitar, D.S.; Ogilvie, R.I. Amantadine kinetics in healthy young subjects after long-term dosing. *Clin. Pharmacol. Ther.* **1979**, *26*, 729–736. [[CrossRef](#)] [[PubMed](#)]
14. Muller, F.; Weitz, D.; Deraud, V.; Sandvoss, M.; Mertsch, K.; Konig, J.; Fromm, M.F. Contribution of MATE1 to renal secretion of the NMDA receptor antagonist memantine. *Mol. Pharm.* **2017**, *14*, 2991–2998. [[CrossRef](#)] [[PubMed](#)]
15. Kooijmans, S.A.; Senyschyn, D.; Mezhiselvam, M.M.; Morizzi, J.; Charman, S.A.; Weksler, B.; Romero, I.A.; Couraud, P.O.; Nicolazzo, J.A. The involvement of a Na(+)- and Cl(-)-dependent transporter in the brain uptake of amantadine and rimantadine. *Mol. Pharm.* **2012**, *9*, 883–893. [[CrossRef](#)] [[PubMed](#)]
16. Goralski, K.B.; Lou, G.; Prowse, M.T.; Gorboulev, V.; Volk, C.; Koepsell, H.; Sitar, D.S. The cation transporters rOCT1 and rOCT2 interact with bicarbonate but play only a minor role for amantadine uptake into rat renal proximal tubules. *J. Pharmacol. Exp. Ther.* **2002**, *303*, 959–968. [[CrossRef](#)]
17. Busch, A.E.; Karbach, U.; Miska, D.; Gorboulev, V.; Akhoundova, A.; Volk, C.; Arndt, P.; Ulzheimer, J.C.; Sonders, M.S.; Baumann, C.; et al. Human neurons express the polyspecific cation transporter hOCT2, which translocates monoamine neurotransmitters, amantadine, and memantine. *Mol. Pharmacol.* **1998**, *54*, 342–352. [[CrossRef](#)]

18. Tachikawa, M.; Takeda, Y.; Tomi, M.; Hosoya, K. Involvement of OCTN2 in the transport of acetyl-L-carnitine across the inner blood-retinal barrier. *Invest. Ophthalmol. Vis. Sci.* **2010**, *51*, 430–436. [[CrossRef](#)]
19. Kubo, Y.; Yamamoto, M.; Matsunaga, K.; Usui, T.; Akanuma, S.I.; Hosoya, K.I. Retina-to-blood transport of 1-methyl-4-phenylpyridinium involves carrier-mediated process at the blood-retinal barrier. *J. Pharm. Sci.* **2017**, *106*, 2583–2591. [[CrossRef](#)]
20. Kubo, Y.; Kusagawa, Y.; Tachikawa, M.; Akanuma, S.; Hosoya, K. Involvement of a novel organic cation transporter in verapamil transport across the inner blood-retinal barrier. *Pharm. Res.* **2013**, *30*, 847–856. [[CrossRef](#)]
21. Kubo, Y.; Shimizu, Y.; Kusagawa, Y.; Akanuma, S.; Hosoya, K. Propranolol transport across the inner blood-retinal barrier: Potential involvement of a novel organic cation transporter. *J. Pharm. Sci.* **2013**, *102*, 3332–3342. [[CrossRef](#)] [[PubMed](#)]
22. Kubo, Y.; Tsuchiyama, A.; Shimizu, Y.; Akanuma, S.; Hosoya, K. Involvement of carrier-mediated transport in the retinal uptake of clonidine at the inner blood-retinal barrier. *Mol. Pharm.* **2014**, *11*, 3747–3753. [[CrossRef](#)] [[PubMed](#)]
23. Han, Y.H.; Sweet, D.H.; Hu, D.N.; Pritchard, J.B. Characterization of a novel cationic drug transporter in human retinal pigment epithelial cells. *J. Pharmacol. Exp. Ther.* **2001**, *296*, 450–457.
24. Hosoya, K.; Tomi, M.; Ohtsuki, S.; Takanaga, H.; Ueda, M.; Yanai, N.; Obinata, M.; Terasaki, T. Conditionally immortalized retinal capillary endothelial cell lines (TR-iBRB) expressing differentiated endothelial cell functions derived from a transgenic rat. *Exp. Eye. Res.* **2001**, *72*, 163–172. [[CrossRef](#)] [[PubMed](#)]
25. Nabi, I.R.; Mathews, A.P.; Cohen-Gould, L.; Gundersen, D.; Rodriguez-Boulan, E. Immortalization of polarized rat retinal pigment epithelium. *J. Cell. Sci.* **1993**, *104*, 37–49. [[CrossRef](#)]
26. Hosoya, K.; Yamamoto, A.; Akanuma, S.; Tachikawa, M. Lipophilicity and transporter influence on blood-retinal barrier permeability: A comparison with blood-brain barrier permeability. *Pharm. Res.* **2010**, *27*, 2715–2724. [[CrossRef](#)]
27. Kubo, Y.; Yamada, M.; Konakawa, S.; Akanuma, S.I.; Hosoya, K.I. Uptake study in lysosome-enriched fraction: Critical involvement of lysosomal trapping in quinacrine uptake but not fluorescence-labeled verapamil transport at blood-retinal barrier. *Pharmaceutics* **2020**, *12*, 747. [[CrossRef](#)] [[PubMed](#)]
28. Tega, Y.; Tabata, H.; Kurosawa, T.; Kitamura, A.; Itagaki, F.; Oshitari, T.; Deguchi, Y. Structural requirements for uptake of diphenhydramine analogs into hCMEC/D3 cells via the proton-coupled organic cation antiporter. *J. Pharm. Sci.* **2021**, *110*, 397–403. [[CrossRef](#)]
29. Lin, H.; Miller, S.S. pHi regulation in frog retinal pigment epithelium: Two apical membrane mechanisms. *Am. J. Physiol.* **1991**, *261*, C132–C142. [[CrossRef](#)]
30. Yamaoka, K.; Tanigawara, Y.; Nakagawa, T.; Uno, T. A pharmacokinetic analysis program (multi) for microcomputer. *J. Pharmacobiodyn.* **1981**, *4*, 879–885. [[CrossRef](#)]
31. Grabowski, T.; Gumulka, S.W.; Borucka, B.; Raszewski, W. Analysis relationships between pharmacokinetic parameters in silico/in vivo of selected antiviral drugs based on structural analysis. *Adv. Clin. Exp. Med.* **2008**, *17*, 285–292.
32. Grundemann, D.; Gorboulev, V.; Gambaryan, S.; Veyhl, M.; Koepsell, H. Drug excretion mediated by a new prototype of polyspecific transporter. *Nature* **1994**, *372*, 549–552. [[CrossRef](#)]
33. Urakami, Y.; Okuda, M.; Masuda, S.; Saito, H.; Inui, K.I. Functional characteristics and membrane localization of rat multispecific organic cation transporters, OCT1 and OCT2, mediating tubular secretion of cationic drugs. *J. Pharmacol. Exp. Ther.* **1998**, *287*, 800–805. [[PubMed](#)]
34. Grundemann, D.; Babin-Ebell, J.; Martel, F.; Ording, N.; Schmidt, A.; Schomig, E. Primary structure and functional expression of the apical organic cation transporter from kidney epithelial LLC-PK1 cells. *J. Biol. Chem.* **1997**, *272*, 10408–10413. [[CrossRef](#)] [[PubMed](#)]
35. Kekuda, R.; Prasad, P.D.; Wu, X.; Wang, H.; Fei, Y.J.; Leibach, F.H.; Ganapathy, V. Cloning and functional characterization of a potential-sensitive, polyspecific organic cation transporter (OCT3) most abundantly expressed in placenta. *J. Biol. Chem.* **1998**, *273*, 15971–15979. [[CrossRef](#)] [[PubMed](#)]
36. Wu, X.; Kekuda, R.; Huang, W.; Fei, Y.J.; Leibach, F.H.; Chen, J.; Conway, S.J.; Ganapathy, V. Identity of the organic cation transporter OCT3 as the extraneuronal monoamine transporter (uptake2) and evidence for the expression of the transporter in the brain. *J. Biol. Chem.* **1998**, *273*, 32776–32786. [[CrossRef](#)]
37. Sloan, J.L.; Mager, S. Cloning and functional expression of a human Na(+) and Cl(-)-dependent neutral and cationic amino acid transporter B(0+). *J. Biol. Chem.* **1999**, *274*, 23740–23745. [[CrossRef](#)] [[PubMed](#)]
38. Nakanishi, T.; Hatanaka, T.; Huang, W.; Prasad, P.D.; Leibach, F.H.; Ganapathy, M.E.; Ganapathy, V. Na+- and Cl--coupled active transport of carnitine by the amino acid transporter ATB(0,+) from mouse colon expressed in HRPE cells and Xenopus oocytes. *J. Physiol.* **2001**, *532*, 297–304. [[CrossRef](#)]
39. Yabuuchi, H.; Tamai, I.; Nezu, J.; Sakamoto, K.; Oku, A.; Shimane, M.; Sai, Y.; Tsuji, A. Novel membrane transporter OCTN1 mediates multispecific, bidirectional, and pH-dependent transport of organic cations. *J. Pharmacol. Exp. Ther.* **1999**, *289*, 768–773.
40. Wu, X.; George, R.L.; Huang, W.; Wang, H.; Conway, S.J.; Leibach, F.H.; Ganapathy, V. Structural and functional characteristics and tissue distribution pattern of rat OCTN1, an organic cation transporter, cloned from placenta. *Biochim. Biophys. Acta.* **2000**, *1466*, 315–327. [[CrossRef](#)]
41. Wu, X.; Huang, W.; Prasad, P.D.; Seth, P.; Rajan, D.P.; Leibach, F.H.; Chen, J.; Conway, S.J.; Ganapathy, V. Functional characteristics and tissue distribution pattern of organic cation transporter 2 (OCTN2), an organic cation/carnitine transporter. *J. Pharmacol. Exp. Ther.* **1999**, *290*, 1482–1492. [[PubMed](#)]

42. Tamai, I.; Ohashi, R.; Nezu, J.; Yabuuchi, H.; Oku, A.; Shimane, M.; Sai, Y.; Tsuji, A. Molecular and functional identification of sodium ion-dependent, high affinity human carnitine transporter OCTN2. *J. Biol. Chem.* **1998**, *273*, 20378–20382. [[CrossRef](#)] [[PubMed](#)]
43. Otsuka, M.; Matsumoto, T.; Morimoto, R.; Arioka, S.; Omote, H.; Moriyama, Y. A human transporter protein that mediates the final excretion step for toxic organic cations. *Proc. Natl. Acad. Sci. USA* **2005**, *102*, 17923–17928. [[CrossRef](#)] [[PubMed](#)]
44. Ohta, K.Y.; Inoue, K.; Hayashi, Y.; Yuasa, H. Molecular identification and functional characterization of rat multidrug and toxin extrusion type transporter 1 as an organic cation/H⁺ antiporter in the kidney. *Drug. Metab. Dispos.* **2006**, *34*, 1868–1874. [[CrossRef](#)] [[PubMed](#)]
45. Ito, S.; Kusuhara, H.; Yokochi, M.; Toyoshima, J.; Inoue, K.; Yuasa, H.; Sugiyama, Y. Competitive inhibition of the luminal efflux by multidrug and toxin extrusions, but not basolateral uptake by organic cation transporter 2, is the likely mechanism underlying the pharmacokinetic drug-drug interactions caused by cimetidine in the kidney. *J. Pharmacol. Exp. Ther.* **2012**, *340*, 393–403. [[CrossRef](#)]
46. Engel, K.; Wang, J. Interaction of organic cations with a newly identified plasma membrane monoamine transporter. *Mol. Pharmacol.* **2005**, *68*, 1397–1407. [[CrossRef](#)]
47. Parsons, C.G.; Panchenko, V.A.; Pinchenko, V.O.; Tsyndrenko, A.Y.; Krishtal, O.A. Comparative patch-clamp studies with freshly dissociated rat hippocampal and striatal neurons on the NMDA receptor antagonistic effects of amantadine and memantine. *Eur. J. Neurosci.* **1996**, *8*, 446–454. [[CrossRef](#)]
48. Nishikawa, N.; Nagai, M.; Moritoyo, T.; Yabe, H.; Nomoto, M. Plasma amantadine concentrations in patients with Parkinson's disease. *Parkinsonism. Relat. Disord.* **2009**, *15*, 351–353. [[CrossRef](#)]